PNAS RESEARCH ARTICLE | GENETICS

Head-tail-head neural wiring underlies gut fat storage in *Caenorhabditis elegans* temperature acclimation

Haruka Motomura[a,b,c,1], Makoto Ioroi[a,b,c], Kazutoshi Murakami[a,b,c], Atsushi Kuhara[a,b,c,d,2], and Akane Ohta[a,b,c,1,2]

Edited by David Denlinger, The Ohio State University, Columbus, OH; received March 2, 2022; accepted June 17, 2022

Animals maintain the ability to survive and reproduce by acclimating to environmental temperatures. We showed here that *Caenorhabditis elegans* exhibited temperature acclimation plasticity, which was regulated by a head-tail-head neural circuitry coupled with gut fat storage. After experiencing cold, *C. elegans* individuals memorized the experience and were prepared against subsequent cold stimuli. The cyclic adenosine monophosphate (cAMP) response element-binding protein (CREB) regulated temperature acclimation in the ASJ thermosensory neurons and RMG head interneurons, where it modulated ASJ thermosensitivity in response to past cultivation temperature. The PVQ tail interneurons mediated the communication between ASJ and RMG via glutamatergic signaling. Temperature acclimation occurred via gut fat storage regulation by the triglyceride lipase ATGL-1, which was activated by a neuropeptide, FLP-7, downstream of CREB. Thus, a head-tail-head neural circuit coordinated with gut fat influenced experience-dependent temperature acclimation.

Caenorhabditis elegans | temperature acclimation | CREB | neuropeptide | neural circuit

Significance

Animals maintain the ability to survive and reproduce by acclimating to temperature. The nematode *Caenorhabditis elegans* possesses experience-dependent temperature acclimation. Here, we revealed that a head-tail-head neural circuit regulated gut fat storage, which was essential for temperature acclimation. The head-tail-head neural circuit comprised ASJ head thermosensory neurons, PVQ tail interneurons, and RMG head hub interneurons, which induced secretion of the neuropeptide FLP-7. FLP-7 was received by its receptor on the intestine, which activated the adipose triglyceride lipase, thus inducing intestinal lipolysis, which is critical for temperature acclimation. The proposed head-tail-head neuronal wiring coupled with gut fat storage provides a useful model for understanding the role of the brain–gut network in the systemic regulation of temperature acclimation.

Environmental conditions continuously change in nature, which means that the ability to adapt provides an evolutionary advantage (1). Temperature is a critical environmental condition that directly affects numerous biological functions. Animal species often detect ambient temperature in a continuous capacity, with detected signals governing physiological activities such as homeostasis, lipid metabolism, and reproduction (2). When thermosensory neurons or temperature-sensitive organs detect a drastic change in temperature, the nervous system and/or downstream tissues undergo systematic changes (2). The simply compact nervous system of the nematode *Caenorhabditis elegans*, with its 302 neurons and complete neural wiring diagram, is well suited for studying the entire system via which sensory information is processed to generate changes in physiological characteristics.

C. elegans possesses cold tolerance, depending on the cultivation temperature (Fig. 1 *A* and *B*) (3–7). Moreover, temperature acclimation, a phenomenon in which animals acclimate to a new temperature in a few hours, has been observed (4, 5). Our previous studies reported that ASJ thermosensory neurons respond to thermal stimuli via the cyclic guanosine monophosphate (cGMP)-gated channels TAX-2/TAX-4 (3). The ASG and ADL sensory neurons also function as thermosensory neurons that regulate cold tolerance and acclimation, in which the mechanoreceptor DEG/ENaC DEG-1 and the transient receptor potential vanilloid (TRPV) channels OSM-9/OCR-1 and -2 act as thermoreceptors (8–10).

The cAMP response element-binding protein (CREB) is a key mediator of long-term memory in the nervous system (11, 12). Nishida et al. reported that CREB, which is encoded by the *crh-1* gene, modulates the activity of the AFD thermosensory neurons in a cell-autonomous manner in *C. elegans* (13). Whether other sensory neurons, such as the ASJ neurons, possess similar CREB-dependent activity remains undetermined.

In this study, genetic and physiological evidence indicated that CREB functions cell autonomously in the ASJ thermosensory neurons to modulate neural excitability in a cultivation-temperature-dependent manner. In the temperature acclimation, ASJ neurons transmitted temperature signals to the PVQ tail interneurons, which in turn, released glutamate to the RMG interneurons located in the head. The RMG interneurons promoted the secretion of a neuropeptide that is received by its receptor in the intestine, which activated triglyceride lipase and then induced fat loss, resulting in cold tolerance control. We propose that this body-wide circuit modulates fat storage for temperature acclimation.

Results and Discussion

***crh-1*, which Encodes CREB, Is Required for Temperature Acclimation.** *C. elegans* displays experience-dependent cold tolerance and temperature acclimation (Fig. 1 *A* and *B*).

Author contributions: H.M., A.K., and A.O. designed research; H.M., M.I., K.M., A.K., and A.O. performed research; H.M., M.I., K.M., A.K., and A.O. analyzed data; and H.M., A.K., and A.O. wrote the paper.

The authors declare no competing interest.

This article is a PNAS Direct Submission.

[1]H.M. and A.O. contributed equally to this work.

[2]To whom correspondence may be addressed. Email: atsushi_kuhara@me.com or o_akaneiro@me.com.

This article contains supporting information online at http://www.pnas.org/lookup/suppl/doi:10.1073/pnas.2203121119/-/DCSupplemental.

Published August 1, 2022.

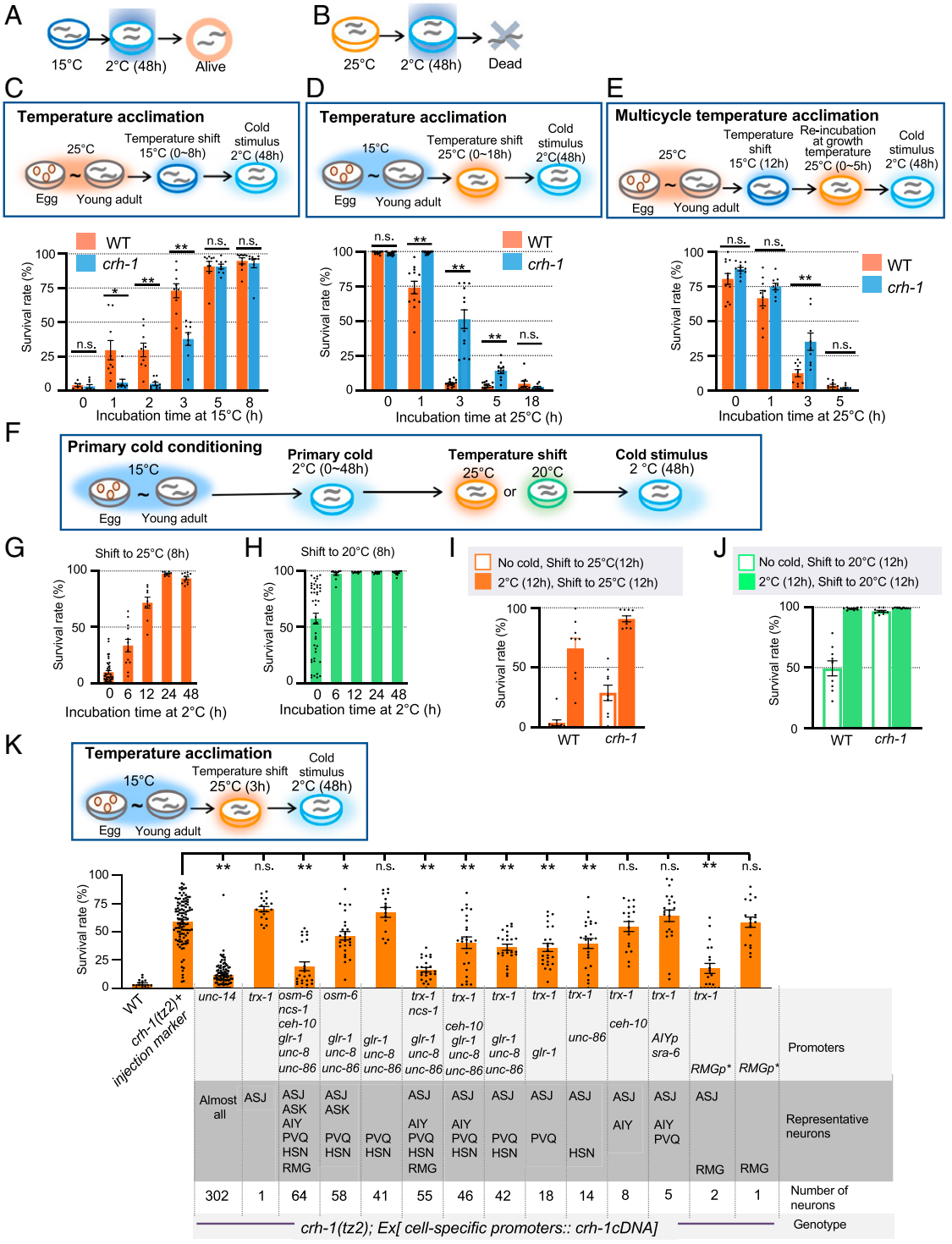

Fig. 1. Temperature acclimation was an experience-dependent cold tolerance regulated by CRH-1. (*A*, *B*) Cold tolerance in wild-type worms. The 15 °C-grown wild-type worms survive at 2 °C (*A*), whereas 25 °C-grown wild-type worms fail to survive at 2 °C (*B*). (*C*, *D*) Temperature acclimation test. (*C*) Animals grown at 25 °C were maintained at 15 °C for 0–8 h, and then exposed to 2 °C. The survival rate of *crh-1* mutants decreased compared with that of wild-type worms when the worms experienced 3 h of incubation at 15 °C. Number of assays, ≥6. The error bars indicate the SEMs. n.s. $P \geq 0.05$; *$P < 0.05$; **$P < 0.01$. (*D*) Animals grown at 15 °C were maintained at 25 °C for 0–18 h, and then exposed to 2 °C. The survival rate of *crh-1* mutants increased compared with that of wild-type worms when the worms experienced 3 h of incubation at 25 °C. Number of assays, ≥9. The error bars indicate the SEMs. n.s. $P \geq 0.05$; *$P < 0.05$; **$P < 0.01$. (*E*) Animals grown at 25 °C were maintained to 15 °C for 12 h, returned to 25 °C for 0–5 h, and then exposed to 2 °C. *crh-1* mutants showed enhanced cold tolerance. Number of assays, ≥9. The error bars indicate the SEMs. n.s. $P \geq 0.05$; *$P < 0.05$; **$P < 0.01$. Comparisons were performed using Welch's *t* tests (*C*–*E*). (*F*–*J*) Primary cold conditioning; 15 °C-grown worms are exposed to a primary cold stimulus at 2 °C (0–48 h) and further cultivated at 25 °C for 8 h (*G*), 20 °C for 8 h (*H*), 25 °C for 12 h (*I*), or 20 °C for 12 h (*J*). Finally, they were exposed to a cold stimulus at 2 °C for 48 h. (*G*, *H*) Survival rate of wild-type worms after primary cold conditioning. Number of assays, ≥9. (*I*, *J*) Survival rate of wild-type and *crh-1* mutant worms at 2 °C for 48 h after a temperature shift from 15 °C to 25 °C (*I*) or to 20 °C (*J*) without or with primary cold conditioning (2 °C, 12 h). Number of assays, ≥9. The error bars indicate the SEMs. (*K*) The abnormal superior survival of *crh-1* mutants that were subjected to the [15 °C → 25 °C (3 h) → 2 °C] protocol was rescued by expressing a *crh-1* cDNA in both ASJ and RMG neurons. *RMGp** indicates that the CRE-LoxP system was used to express the *crh-1* cDNA in RMG neurons (refer to "Molecular Biology" in the *Methods* section of the *SI Appendix*). Number of assays, ≥15. The error bars indicate the SEMs. n.s. $P \geq 0.05$; *$P < 0.05$; **$P < 0.01$. Comparisons with *crh-1(tz2)* + injection marker were performed using one-way ANOVA followed by Dunnett's post hoc test.

The 15 °C-grown wild-type (N2) individuals were able to survive cold stimuli for 48 h at 2 °C (Fig. 1*A*); however, 25 °C-grown animals were not (Fig. 1*B*) (3, 5–7). We reported previously that temperature acclimation is the ability to adapt to an altered temperature within a few hours (4). For example, after wild-type animals grown at 15 °C were maintained at 25 °C for 3 h and then exposed to a cold stimulus (15 °C → 25 °C [3 h]→ 2 °C), they could not survive (4).

Because CREB is involved in preferential temperature seeking (13–15), we investigated the role of the *C. elegans* CREB homolog (*crh-1*) gene, which encodes CREB, in temperature acclimation. To detect abnormalities in *crh-1* mutants, we used the [25 °C → 15 °C → 2 °C] and [15 °C → 25 °C → 2 °C] protocols (Fig. 1 *C* and *D*). The results of these experiments showed differences in the rates of acclimation between wild-type and *crh-1* mutant animals (Fig. 1 *C* and *D*), which indicates that CRH-1 facilitates acclimation within the first 3 h after exposure to a temperature change.

In addition, we examined the plasticity of temperature acclimation using *crh-1* mutants and wild type, because CREB is involved in long-term memory formation (11, 12). The cold-tolerant state was reversibly changed by a multicycle temperature acclimation assay (Fig. 1*E*). When 25 °C-grown animals were transferred to 15 °C for 12 h, they survived at 2 °C [25 °C → 15 °C (12 h) → 25 °C (0 h) → 2 °C] (Fig. 1*E*). In contrast, if 25 °C-grown animals were transferred to 15 °C for 12 h and returned to 25 °C for 3 h, they died at 2 °C [25 °C → 15 °C (12 h) → 25 °C (3 h) → 2 °C] (Fig. 1*E*). *crh-1* mutants showed abnormal phenotypes under the same protocol (Fig. 1*E*).

We investigated the effects of primary cold conditioning on survival after a second cold stimulus (Fig. 1 *F*–*H*). When 15 °C-cultivated animals without primary cold conditioning were transferred to 25 °C for 8 h, they could not survive at 2 °C [15 °C → 2 °C (0 h) → 25 °C (8 h) → 2 °C] (Fig. 1*G*). However, when 15 °C-cultivated animals with primary cold conditioning for 48 h were transferred to 25 °C for 8 h, they could then survive at 2 °C [15 °C → 2 °C (48 h) → 25 °C (8 h) → 2 °C] (Fig. 1*G*). These findings indicate that animals may record their first cold experience and that this record increases cold tolerance in 25 °C-cultivated animals. This phenomenon varied, depending on the length of the primary cold conditioning [15 °C → 2 °C (6, 12, 24, or 48 h) → 25 °C (8 h) → 2 °C] (Fig. 1*G*) and on the second cultivation temperature used after the primary cold conditioning [15 °C → 2 °C (6, 12, 24, or 48 h) → 20 °C or 15 °C (8 h) → 2 °C] (Fig. 1*H* and *SI Appendix*, Fig. S1*A*).

In the temperature shift assay from 15 °C to 25 °C with primary cold conditioning [15 °C → 2 °C (12 h) → 25 °C (12 h) → 2 °C] (Fig. 1*I*), ∼60% of wild-type animals survived (Fig. 1*I*); conversely, using the same temperature shift without the primary cold conditioning [15 °C → 2 °C (0 h) → 25 °C (12 h) → 2 °C] (Fig. 1*I*), most of the wild-type animals died (Fig. 1*I*). We found that *crh-1* mutants showed an abnormally enhanced cold tolerance phenotype after the same temperature shifts (Fig. 1*I*). A similar abnormal phenotype of the *crh-1* mutants was observed under the [15 °C → 2 °C (0 h) → 20 °C (12 h) → 2 °C] (Fig. 1*J*) protocol, whereas *crh-1* mutants showed phenotypes similar to those of wild-type animals under the [15 °C → 2 °C (12 h) → 15 °C (12 h) → 2 °C] protocol (*SI Appendix*, Fig. S1*B*).

CREB Functions in ASJ Sensory Neurons and RMG Interneurons to Enable Rapid Temperature Acclimation. The abnormal temperature acclimation of *crh-1* mutants was restored by expressing the *crh-1* cDNA in almost all neurons using an *unc-14* promoter (*unc-14p*; Fig. 1*K*). Next, we simultaneously used six promoters (*osm-6p*, *ncs-1p*, *ceh-10p*, *glr-1p*, *unc-8p*, and *unc-86p*) or five promoters (*trx-1p*, *ncs-1p*, *glr-1p*, *unc-8p*, and *unc-86p*) to express the *crh-1* cDNA in *crh-1* mutants, and these transgenic worms showed a fully recovered phenotype (Fig. 1*K*, *crh-1(tz2); Ex[(osm-6p, ncs-1p, ceh-10p, glr-1p, unc-8p, unc-86p)::crh-1 cDNA]* and *crh-1(tz2); Ex[(trx-1p, ncs-1p, glr-1p, unc-8p, unc-86p)::crh-1 cDNA]*). These results in combination with some of the six promoters and/or the *trx-1* promoter led us to hypothesize that simultaneous expression of CRH-1 in ASJ and RMG neurons is required for temperature acclimation. Simultaneous expression of CRH-1 in both the ASJ and RMG neurons in *crh-1* mutants resulted in the rescue of abnormality (Fig. 1*K*, *crh-1(tz2); Ex[(trx-1p and RMGp)::crh-1 cDNA]*: 17.5%), whereas CRH-1 expression in the ASJ or RMG neurons alone did not rescue the phenotype. These results indicate that CRH-1 promotes temperature acclimation in ASJ sensory neurons and RMG interneurons.

ASJ Thermosensory Neurons Modulate the Response to Temperature Stimuli Depending on the Cultivation Temperature. ASJ thermosensory activity changes depending on the worm cultivation temperature (3). To elucidate the physiological basis of this function, we measured ASJ activity via the cameleon Ca^{2+} indicator during extended warmth stimulation. ASJ Ca^{2+} concentrations in both 20 °C- and 23 °C-cultivated wild-type animals increased until the temperature reached 20 °C (Fig. 2*A*). In 23 °C-cultivated animals, a continuous, oscillatory ASJ Ca^{2+} concentration increase was observed from 16.5 °C to 24 °C, peaking at 23 °C (Fig. 2*A*). The oscillatory Ca^{2+} increase also peaked at 20 °C in 20 °C-cultivated animals (Fig. 2*A*), whereas Ca^{2+} in 15 °C-cultivated animals did not continuously increase under a warm stimulus (Fig. 2 *B*, *E*, and *H*). Similar ASJ responses were observed in *snb-1* mutants lacking SNB-1/synaptobrevin, which is a protein that is necessary for synaptic vesicle membrane fusion (Fig. 2 *C* and *D*) (16). These results indicate that the maximum change in ASJ Ca^{2+} concentration is dependent on the cultivation temperature in a cell-autonomous manner.

The *crh-1* mutants displayed an abnormal decrease in the peak oscillatory Ca^{2+} increase when cultivated at 20 °C and 23 °C (Fig. 2 *F* and *G*). This decrease was rescued by the expression of the *crh-1* cDNA in ASJ neurons (Fig. 2 *F*, *G*, *I*, and *J*), which indicated that the temperature response in *crh-1* mutants may be down-regulated in ASJ neurons in higher temperature regions. In turn, this may weaken ASJ activity in *crh-1* mutants, which could be why the *crh-1* mutant required a longer time to acclimate.

PVQ Interneurons Bridge ASJ Thermosensory Neurons and RMG Interneurons. CRH-1/CREB regulated ASJ- and RMG-mediated temperature acclimation, despite the absence of a direct chemical or electrical connection between the two (Fig. 2*K*) (17). A previous electron microscopy analysis revealed the presence of a potential interneuron bridge between the ASJ and RMG neurons, with PVQ, ASK, and HSN neurons being candidates because the ASJ neurons lack gap junctions (17). Another study found that the trimeric G protein α subunit, Gαs (Q227L), induces interneuronal hyperactivation (18). We found that Gαs (Q227L) overexpression in various wild-type interneurons driven by the *glr-1* promoter induced an increasingly abnormal temperature acclimation (*SI Appendix*, Fig. S1*E*). Of the cells activated using the *glr-1* promoter, the PVQ interneurons directly synapsed downstream of ASJ (17).

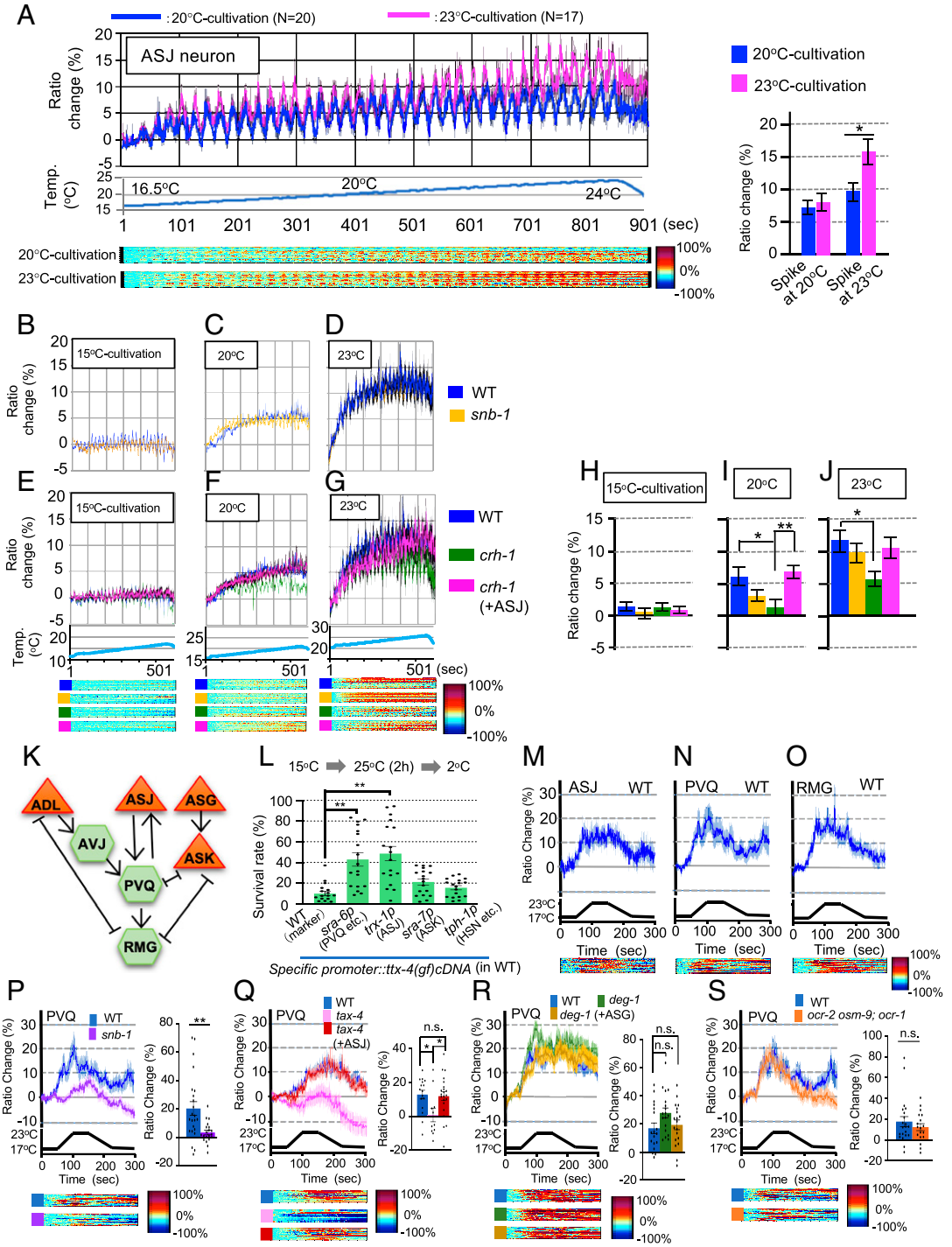

Fig. 2. The neural circuit from ASJ to RMG with intermediate PVQ neurons transmitting temperature signaling. (*A*) ASJ neuron Ca^{2+} imaging of 20 °C- and 23 °C-cultivated wild-type animals in response to defined temperature stimuli. The graph indicates the yellow/cyan fluorescent protein (YFP/CFP) ratio change during moderate warming stimuli with oscillation. The bar graph indicates the average ratio change over 3 s, which included 1 s before and 1 s after the spike peak after reaching 20 °C or 23 °C. The bar graph color key is the same for the corresponding response curve. The error bars indicate the SEMs. **P* < 0.05; ***P* < 0.01. (*B–D*) ASJ neuron Ca^{2+} imaging of 15 °C-, 20 °C-, and 23 °C-cultivated wild-type worms and *snb-1* mutants lacking synaptobrevin in response to defined temperature stimuli. *snb-1* mutants showed normal phenotypes. (*E–G*) ASJ neuron Ca^{2+} imaging of 15 °C(E)-, 20 °C(F)-, and 23 °C(G)-cultivated wild-type, *crh-1* mutant, and ASJ-rescued *crh-1* mutant (*crh-1;Ex[trx-1p::crh-1 cDNA]*) worms. The abnormal temperature response was rescued in transgenic animals. Data from wild-type animals cultivated at 15 °C, 20 °C, and 23 °C, as shown in *B–D*, are shared by *E–G*, respectively, because the experiments were conducted simultaneously. (*H–J*) The bar graphs indicate the average ratios of change from 411 to 421 s (*H*), 510 to 520 s (*I*), and 446 to 456 s (*J*). The bar graph and heatmap color keys are the same for the corresponding response curve. Number of tests, ≥19. The error bar indicates the SEM. **P* < 0.05; ***P* < 0.01. (*K*) Neural circuit between ASJ and RMG neurons. (*L*) The temperature acclimation of wild-type animals expressing the constitutively active form of PKC (*ttx-4gf*) in ASJ or PVQ neurons was abnormal. Number of assays, ≥18. The error bars indicate the SEMs. ***P* < 0.01. (*M–O*) Ca^{2+} imaging in ASJ (*M*), PVQ (*N*, *P–S*), and RMG (*O*) neurons in 23 °C-cultivated worms of each strain in response to defined temperature stimuli. *tax-4* (+ASJ) (*Q*) and *deg-1* (+ASG) (*R*) indicate the ASJ-rescued *tax-4* mutant (*tax-4;Ex[trx-1p::tax-4 cDNA]*) and the ASG-rescued *deg-1* mutant (*deg-1; Ex[gcy-21p::deg-1cDNA]*), respectively. The YFP/CFP ratio change was detected by yellow cameleon. Each row in the heatmaps represents images cropped from one worm, and excluded values over 100% are shown in black. The bar graph and heatmap color keys are the same for the corresponding response curve. Part of the data from wild-type animals shown in *N*, *P*, and *S* are shared because some of the experiments were conducted simultaneously. The bar graphs indicate the average ratio of change over 103–107 (*P*, *S*), 150–180 (*Q*), and 99–103 (*R*) s. Number of animals, ≥11. The error bars indicate the SEMs. n.s. *P* ≥ 0.05; **P* < 0.05; ***P* < 0.01. Comparisons were performed using Welch's *t* tests (*A*, *P*, *S*) or one-way ANOVA followed by Tukey-Kramer tests (*H–J*, *Q*, *R*) or Dunnett's post hoc tests (*L*).

Using PKCgf/TTX-4gf, a constitutively active form of protein kinase C (PKCgf), which enhances neuropeptide release at presynaptic dense-core vesicles (19), we found an abnormally enhanced temperature acclimation in worms expressing PKCgf in wild-type PVQ neurons (*sra-6p*; Fig. 2*L*) and ASJ thermosensory neurons (*trx-1p*; Fig. 2*L*). In contrast, PKCgf expression in downstream neurons, such as ASK (*sra-7p*; Fig. 2*L*) or HSN (*tph-1p*; Fig. 2*L*), did not markedly affect temperature acclimation. These findings are consistent with the normal phenotype observed in *tph-1* and *mod-1* mutants, which sustain impaired serotonin synthesis in HSN and dysfunctional serotonin receptors in HSN-downstream cells, respectively (*SI Appendix*, Fig. S1*D*) (20, 21). Although PVQ neurons are developmental guide interneurons for constructing neural connections to other neurons during the embryonic stage (22), the role of PVQ neurons in neural circuits underlying specific sensory responses has not been demonstrated.

To investigate whether PVQ and RMG are involved in temperature signaling, we conducted calcium imaging for these interneurons (Fig. 2 *N* and *O*). The activity of PVQ and RMG neurons was altered under temperature stimuli in a fashion similar to that observed in the ASJ thermosensory neurons (Fig. 2 *M*–*O*). Calcium imaging revealed that the ASJ temperature signals traveled toward the PVQ and RMG interneurons.

PVQ Interneurons Are Regulated by ASJ Thermosensory Neurons. To investigate whether PVQ interneurons are activated via neural signaling from upstream neurons with synaptic connections, we performed calcium measurements in the PVQ neurons of mutants defective in SNB-1 (16). The calcium fluctuation in PVQ neurons during the thermal stimulus was decreased in *snb-1* mutants (Fig. 2*P*), which indicated that PVQ neurons are activated by a neural signaling from upstream neurons through synapses.

To identify the upstream sensory neurons that activate PVQ interneurons, we monitored the Ca^{2+} concentration of PVQ neurons in the mutants with impaired ASJ, ADL, and ASG thermosensory neurons, which are essential for cold tolerance (3, 8, 10, 23). The temperature-responsive Ca^{2+} levels in PVQ were decreased in the ASJ-defective mutant *tax-4*, which lacks a cGMP-gated channel (Fig. 2*Q*) (3). Moreover, this abnormality was rescued by specifically expressing a *tax-4* cDNA in ASJ neurons (Fig. 2*Q*). These findings indicate that temperature signals from ASJ neurons positively regulate PVQ neurons. Moreover, the PVQ neuron Ca^{2+} concentrations of the ASG-defective mutant *deg-1* and ADL-defective mutants *ocr-2 osm-9; ocr-1* were similar to those of wild-type animals (Fig. 2 *R* and *S*). These findings demonstrate that PVQ interneurons are mainly regulated by ASJ thermosensory neurons in temperature signaling.

Glutamatergic PVQ Regulates Temperature Acclimation. The PVQ interneurons are glutamatergic neurons (24), and a modest delay in temperature acclimation was found in *eat-4* mutants lacking the vesicular glutamate transporter (VGLUT) (Fig. 3*A*), which is necessary for presynaptic glutamatergic neurotransmission (25). We found that the abnormal *eat-4* mutant temperature acclimation was rescued by expressing an *eat-4* cDNA in PVQ neurons (Fig. 3*A*), and that PVQ-specific knockdown of *eat-4* in wild-type animals caused an abnormal temperature acclimation similar to that observed in *eat-4* mutants (Fig. 3*B*). These findings demonstrate that EAT-4 in PVQ neurons is necessary for temperature acclimation.

To identify a glutamate receptor for EAT-4-mediated PVQ neuron glutamatergic signaling, we examined the temperature acclimation of mutants lacking expression of glutamate receptors in downstream neurons of PVQ neurons (26–28). We found that several glutamate receptor mutants showed abnormal delays in temperature acclimation (Fig. 3*C*), especially *glr-4* and *glr-5*; these genes are expressed in RMG interneurons (29). We found that knockdown of *glr-4* and *glr-5* in RMG neurons of wild-type animals caused abnormally increased survival rates during cold acclimation (Fig. 3*D*), and that *glr-4, 5* knockdown in RMG neurons also induced a decreased Ca^{2+} response in RMG neurons during exposure to high temperatures (Fig. 3*E*). Thus, GLR-4, -5 appear to play roles in the cold acclimation facilitated by RMG interneurons.

To investigate downstream transmission pathways other than glutamate in PVQ neurons, we found that mutants lacking gap junction innexin showed an abnormal increase in cold tolerance [15 °C → 25 °C (3 h) → 2 °C (48 h)] (Fig. 3*F*). UNC-7 and UNC-9, as hemichannels, are expressed in various neurons, including PVQ neurons (30); however, INX-9, -19 are not expressed in the ASJ, PVQ or RMG neurons (30). *unc-7* and *unc-9* knockdown in PVQ neurons of wild-type animals induced a slightly abnormal temperature acclimation (Fig. 3*G*), which indicates that gap junctions play a minor role in the circuit.

A Secretion Molecule, FLP-7, Affects Temperature Acclimation via Intestinal Fat Loss. A previous report suggested that the cold tolerance status is related to fatty acid metabolism (31). In nutrition and metabolism, a neuropeptide, FLP-7, released from a head neuron is received by its receptor, NPR-22, in the intestine, which alters gut fat storage (32). We found that the *flp-7* and *npr-22* mutants showed an abnormal delay in temperature acclimation (Fig. 4*A*), and this phenotype was similar to that of *flp-7* mutants with knockdown of the glutamate receptor *glr-4*, *-5* in RMG neurons (Fig. 4*B*); this was consistent with a model in which FLP-7 controls temperature acclimation downstream of RMG neurons.

The activation of *adipose triglyceride lipase-1* (*atgl-1*) is linked to intestinal lipolysis and decreased fat storage (33). However, a previous report on cold tolerance and fat mobilization reported that ATGL-1 is not involved in long-term survival under low temperatures (4 °C) regulated by fat mobilization via the hormone-sensitive lipase HOSL-1 (34). Therefore, we measured the expression levels of *atgl-1::GFP* in the intestine of wild-type animals under various cultivation temperatures; its expression was increased in 25 °C-cultivated wild-type compared with 15 °C-cultivated wild-type worms (Fig. 4 *C* and *D*). These findings demonstrate that the fat storage decrease caused by ATGL-1 lipase may be activated in wild-type animals grown at a higher temperature (25 °C).

Intestinal fat storage can be detected by staining with the oil red O (ORO) dye (35). Gut fat storage in 25 °C-cultivated wild-type animals was lower than that of 15 °C-cultivated wild-type animals (Fig. 4 *E* and *F*). A temperature-dependent gut fat alteration was not found in the *flp-7* (neuropeptide) and *npr-22* (receptor) mutants, and *flp-7; npr-22* double mutants showed similar abnormalities to those of the single mutants (Fig. 4*F*); this indicates that the FLP-7 to NPR-22 pathway is involved in gut fat loss at high temperatures.

In *crh-1* mutants, the gut fat storage in 15 °C- and 25 °C-cultivated animals did not differ (Fig. 4*G*, *crh-1*), and this abnormality was rescued by the expression of a *crh-1* cDNA in ASJ and RMG neurons (Fig. 4*G*; *crh-1; Ex[ASJp, RMGp::crh-1cDNA]*). Expressing a *crh-1* cDNA in ASJ and RMG neurons in *crh-1* mutants also rescued the *crh-1* abnormal temperature acclimation

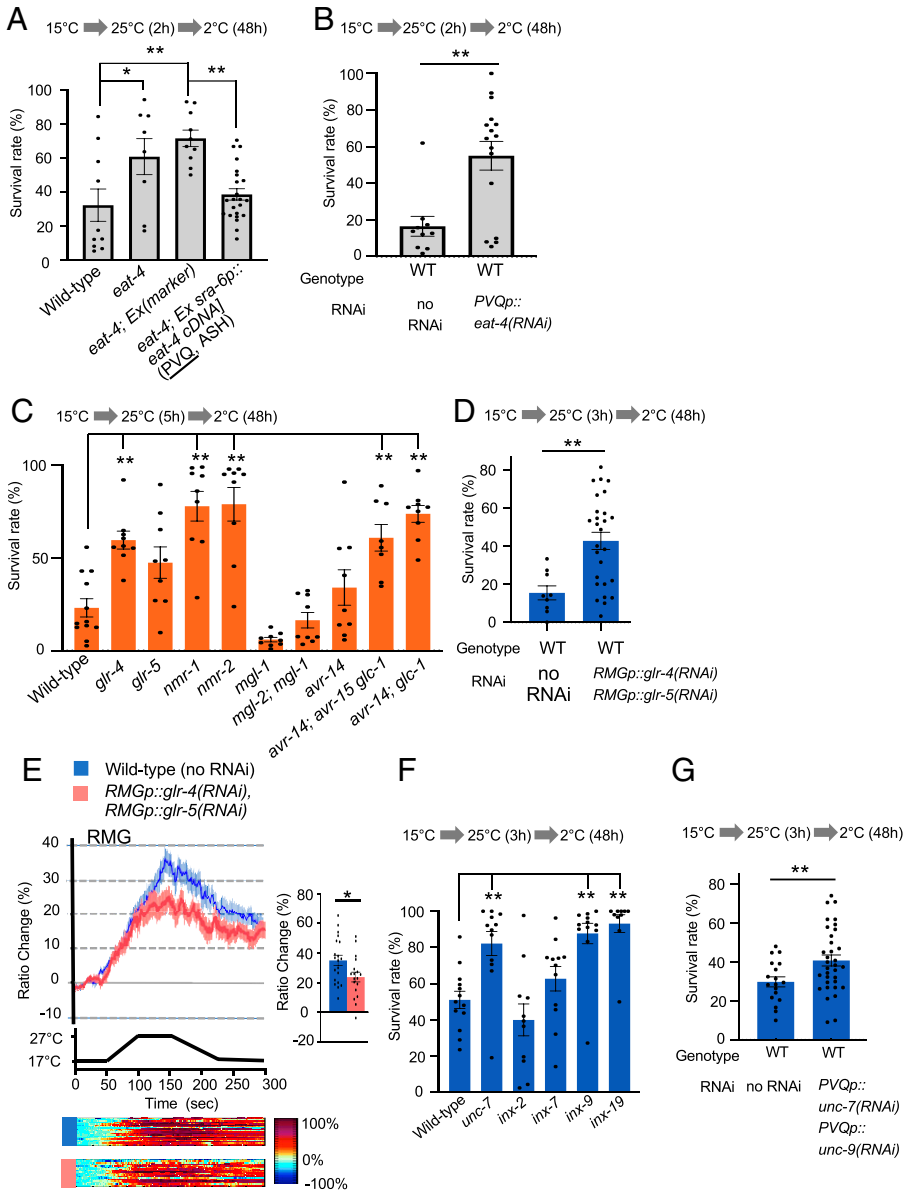

Fig. 3. The head-to-tail temperature acclimation neural circuit is regulated by glutamate signaling. (*A*) The abnormal temperature acclimation of *eat-4* mutants lacking VGLUT was rescued by expressing EAT-4 in PVQ and other neurons. Number of assays, ≥8. The error bars indicate the SEMs. $*P < 0.05$; $**P < 0.01$. (*B*) PVQ-specific knockdown of *eat-4* caused abnormal temperature acclimation. Number of assays, ≥10. The error bars indicate the SEMs. $**P < 0.01$. (*C*) Temperature acclimation of mutants defective in the glutamate receptor. Number of assays, ≥8. The error bar indicates the SEM. $**P < 0.01$. (*D*) The RMG-specific knockdown of *glr-4* and *glr-5* caused abnormal temperature acclimation. Number of assays, ≥9. The error bars indicate the SEMs. $**P < 0.01$. (*E*) Ca^{2+} imaging of RMG neurons in 15 °C-grown animals with *glr-4* and *glr-5* knockdown in RMG neurons. The YFP/CFP ratio change was detected by yellow cameleon. The bar graphs indicate the average ratio of change in 142–146 s. Number of animals, ≥18. The error bars indicate the SEMs. $*P < 0.05$. (*F*) Temperature acclimation of innexin mutants. Number of assays, ≥ 10. The error bars indicate the SEMs. $**P < 0.01$. (*G*) PVQ-specific knockdown of *unc-7* and *unc-9* slightly affected temperature acclimation. Number of assays, ≥18. $**P < 0.01$. Comparisons were performed using Welch's *t* tests (*B*, *D*, *E*, *G*) or one-way ANOVA followed by the Tukey-Kramer test (*A*) or Dunnett's post hoc test (*C*, *F*).

(Fig. 1*K*); therefore, both temperature acclimation and temperature-dependent gut fat loss were controlled by CREB CRH-1 in the neural circuit from ASJ to RMG. In addition, *crh-1; flp-7* double mutants showed similar abnormalities in gut fat loss as did the single mutants (Fig. 4*G*), which implies that FLP-7 promotes lipolysis in the gut downstream of CREB CRH-1.

To summarize the results of these physiological and genetic examinations, the RMG receives temperature signaling from ASJ neurons via PVQ neurons. The RMG neurons promote the secretion of the neuropeptide FLP-7, which is received by its receptor, NPR-22, in the intestine; this accelerates the decrease in gut fat content via ATGL-1, which results in decreased cold tolerance after growth at a high temperature (25 °C) (Fig. 4*H*). The regulatory mechanisms revealed using *C. elegans* in this study may represent conserved long-term adaptive strategies in higher organisms.

Materials and Methods

Strains. *C. elegans* was grown under standard conditions. The N2 (Bristol) strain was used as the wild-type strain in all of the experiments. The following strains were used: *crh-1(tz2), snb-1(md247), eat-4(ky5), tax-4 (p678), ocr-2 (ak47) osm-9 (ky10); ocr-1 (ak46), deg-1 (u38), glr-4(tm3239), glr-5(tm3506), nmr-1(ak4), nmr-2(ok3324), mgl-1(tm1811), mgl-2(tm355); mgl-1(tm1811), avr-14(ad1305), avr-14(ad1305); avr-15(vu227) glc-1(pk54), avr-14(ad1302); glc-1(pk54), unc-7(e5), inx-2(ok376), inx-7(ok2319), inx-9(ok1502), inx-19(ky634), npr-22(tm8953), npr-22(ok1598), flp-7(ok2625), npr-22(ok1598); flp-7(ok2625), crh-1(tz2); flp-7(ok2625), and VS20(hjIs67)[atgl-1p::atgl-1::GFP+mec-7::RFP].*

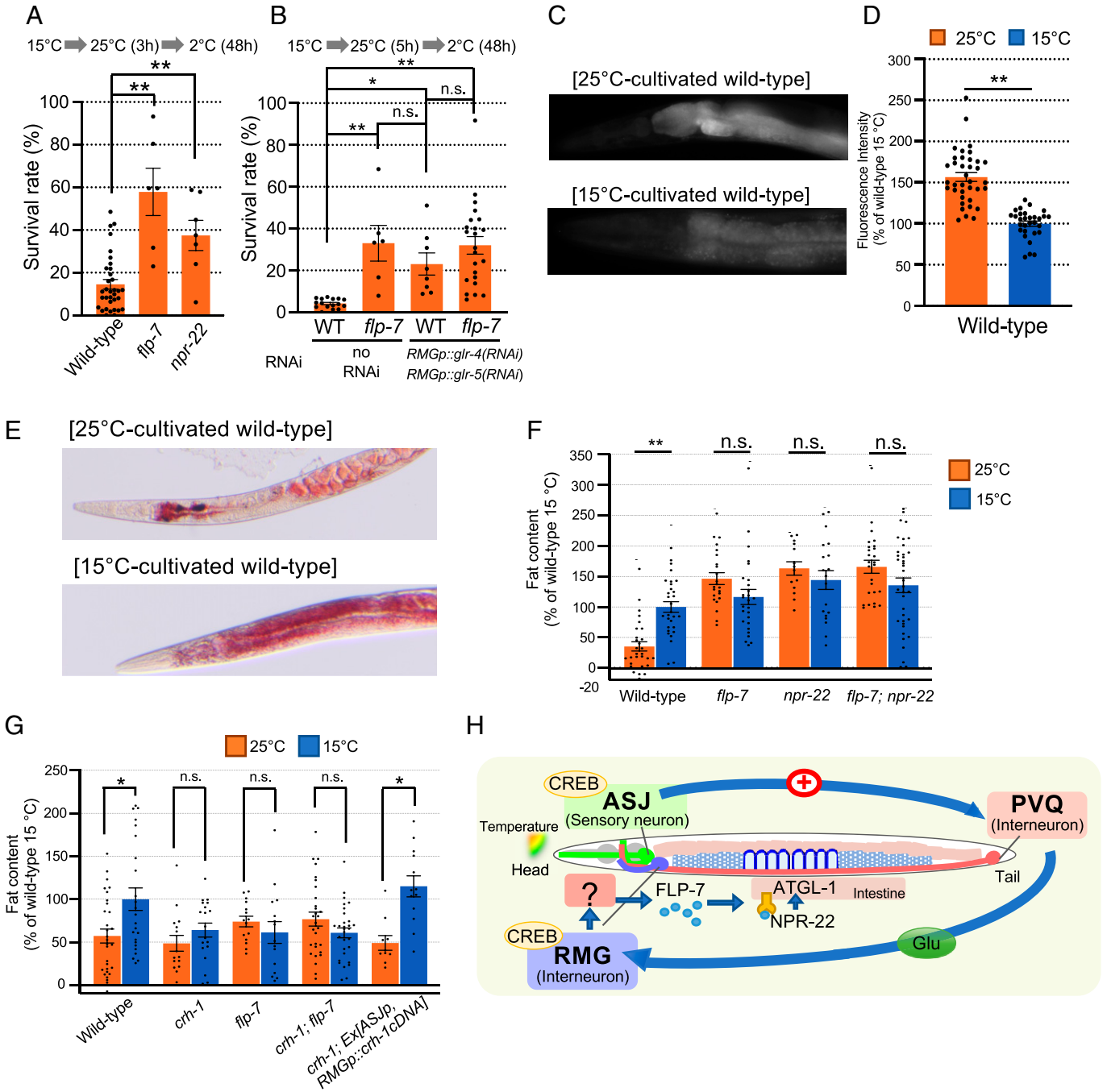

Fig. 4. Intestinal fat accumulation is affected by cultivation temperature through a neuropeptide. (*A*) The *flp-7* and *npr-22* mutants showed abnormal temperature acclimation. Number of assays, ≥ 6. The error bar indicates the SEM. $^{**}P < 0.01$. (*B*) Temperature acclimation of wild-type and *flp-7* mutant worms with *glr-4* and *glr-5* knockdown in RMG interneurons. Number of assays, ≥6. The error bars indicate the SEMs. $^{*}P < 0.05$. $^{**}P < 0.01$. (*C*, *D*) Expression levels of *atgl-1::GFP* in 15 °C- and 25 °C-cultivated wild-type worms. Number of animals, ≥30. The error bars indicate the SEMs. $^{**}P < 0.01$. (*E*) Representative image of Oil Red O (ORO)-stained wild-type animals cultivated at 15 °C or 25 °C. (*F*, *G*) Intestinal fat contents of wild-type and respective mutant worms stained by ORO. The fat content value in each bar is a relative value to the average of 15 °C-cultivated wild-type worms. Number of animals, ≥ 10. The error bars indicate the SEMs. $^{*}P < 0.05$; $^{**}P < 0.01$. Comparisons were performed using Welch's *t* tests (*D*) or one-way ANOVA followed by Dunnett's post hoc test (*A*) or Tukey-Kramer tests (*B*, *F*, *G*). (*H*) Model of the head-to-tail temperature acclimation neural circuit affecting intestinal fat accumulation. Warming stimuli detected by ASJ head sensory neurons activate PVQ tail interneurons; then, PVQ neurons transmit glutamate signaling to RMG head interneurons, which promotes the secretion of the neuropeptide FLP-7 from an unidentified neuron. FLP-7 is received by its receptor, NPR-22, in the intestine, thus inducing fat loss via the activation of the triglyceride lipase ATGL-1, which results in decreased cold tolerance.

Temperature Acclimation Assay. The temperature acclimation assay was conducted based on a previous report (4). Worms were cultured under well-fed conditions on nematode growth media plates, which consist of 2% (wt/vol) agar plates in 3.5-cm-diameter plastic dishes inoculated with *Escherichia coli* OP50. One or more well-fed adult(s) (P_0) were placed on a plate at the experimental temperature for a 15 to 20 hours incubation period, which was terminated once ~100 eggs were laid. P_0 adults were then removed to synchronize growth. Progeny were incubated from egg to adulthood at the initial (cultivating) temperature. At the 15 °C cultivation temperature, progeny were cultured for 5 or 6 day; at the 25 °C cultivating temperature, progeny were cultured for 60–72 h.

When animals reached adulthood, assay plates were transferred to a second (conditioning) temperature environment. After incubation at the conditioning temperature, plates were immediately chilled on ice for 20 min and then transferred to a 2 °C refrigerator (CRB-41A, Hitachi, Japan) for 48 h. After 48 h at

2 °C, assay plates were incubated at 15 °C for 1 d. The number of living and dead worms was then counted. Each assay was performed at least three times.

Multicycle Temperature Acclimation Assay. In this assay, worms were grown under the same conditions as in the temperature acclimation assay. The 25 °C-grown worms in the young adult stage were transferred and incubated at 15 °C for 12 h. Subsequently, they were returned to 25 °C and maintained at that temperature for various periods (0, 1, 3, or 5 h). Finally, worms were exposed to a cold stimulus at 2 °C for 48 h.

Temperature Acclimation Assay with Primary Cold Conditioning. In this assay, worms were grown under the same conditions as in the temperature acclimation assay. The 15 °C-grown worms in the young adult stage were exposed to a primary cold stimulus at 2 °C for 0–48 h. Subsequently, worms were further cultivated at 15 °C, 20 °C, or 25 °C for 8 or 12 h. Finally, they were exposed to a cold stimulus at 2 °C for 48 h.

Statistical Analysis. The cold acclimation tests were performed on more than six plates and on at least three different days. The data values for each experiment are shown as dots in bar graphs. The error bars indicate the SEM. The statistical analyses presented in bar graphs were performed using unpaired Welch's *t* tests to compare two groups, and one-way ANOVA followed by Dunnett's post hoc test or the Tukey-Kramer test for multiple comparisons. Single (*) and double (**) asterisks indicate $P < 0.05$ and $P < 0.01$, respectively. These tests were performed using Mac statistical analysis version 3 (Esumi, Japan). See the *SI Appendix* for additional details on raw data and statistical figures.

In Vivo Calcium Imaging. Animals were glued to a 2% (wt/vol) agar pad on a glass slide and immersed in M9 buffer under a cover glass. The relative changes in intracellular Ca^{2+} concentrations were measured as changes in the acceptor/donor YC fluorescence ratio. Yellow cameleon (YC) fluorescence was simultaneously captured using an EVOLVE512 EM-CCD (charged-coupled device) camera with dual-view (Photometrics, USA), an iXonUltra888 EM-CCD camera with CSU-W1 (Andor, UK), or an ORCA fusion camera with W-view (Hamamatsu Photonics, Japan). Band-pass filters for all YC experiments were used as described in previous reports (3, 8–10, 36, 37). See the *SI Appendix* for additional details.

RNA Interference (RNAi) in Specific Neurons. Transgenic introduction of RNAi in specific neurons was performed as described previously (38). The sense and antisense sequences of the gene used for RNAi were amplified according to the clones in Ahringer's library (39). Cell-specific promoters were fused with gene fragments cloned in the sense and antisense directions. See the *SI Appendix* for additional details.

ORO Staining. ORO staining was performed as reported previously (35). Worms were synchronized and cultivated at a constant temperature; then, day 1 adult worms were harvested and washed 3 times in 1× phosphate-buffered saline (PBS) (pH 7.4). To permeabilize worms, 120 µL PBS and an equal volume of 2× modified Ruvkun's witches brew buffer (160 mM KCl, 40 mM NaCl, 14 mM Na_2EGTA, 1 mM spermidine-HCl, 0.4 mM spermine, 30 mM Na-Pipes, pH 7.4, and 0.2% b-mercaptoethanol) containing 2% paraformaldehyde were added and gently rocked for 1 h. After removal of the permeabilizing buffer, worms were washed with 1× PBS. For dehydration, 1.0 mL of 60% isopropanol was added and allowed to incubate for 15 min. An ORO stock solution (1% ORO-containing isopropanol) was equilibrated for several days, diluted to 60% with water, rocked for 1 h, and then filtered with a 0.22-mm filter. After dehydration, the 60% isopropanol was removed, 1 mL of ORO staining solution was added, and worms were incubated with rotation. Subsequently, the ORO solution was removed, and worms were washed 3 times with 1.0 mL of 1× PBS containing 0.01% Triton X-100. Finally, worms were mounted, and bright-field images were acquired using a Canon color CCD camera.

Image Acquisition and Quantification. All ORO-stained images were acquired under identical settings and exposure times. ORO fluorescence was acquired from the color images using MetaMorph version 7.8 (Molecular Devices, USA) for each animal, and quantified by inverting the red channel intensity and subtracting the inverted value of the mock worm. The mean ORO fluorescence intensities per animal were estimated as the total intensity within an enclosed area of the second and third pairs of intestinal cells.

Quantification of ATGL-1::GFP Fluorescent Images. Quantification of ATGL-1::GFP fluorescence was performed as reported previously (32). Fluorescent images were captured by the MetaVue software version 7.10 (Molecular Devices) using a 20× objective lens on an Olympus IX81 microscope with a monochrome CCD camera. The mean ATGL-1::GFP fluorescent intensities per animal were estimated as the total intensity within an enclosed area of the second and third pairs of intestinal cells.

Data Availability. All of the study data are included in the article and/or supporting information.

ACKNOWLEDGMENTS. We thank I. Mori, Y. Iino S., Mitani, H. Kagoshima, S. Srinivasan, C. Bargmann, S. Xu, and J. Dent for sharing DNA constructs and strains; the National Bioresource Project (Japan) and the *Caenorhabditis* Genetic Center for strains; and S. Fuji, T. Inoue, T. Ishiwari, and K. Kanai for supporting experiments and discussion. We thank Mallory Eckstut and Eric Odle for English editing and proofreading the manuscript. A.K. and A.O. were supported by the Kinoshita Memorial Foundation, Naito Foundation, Takeda Science Foundation, Suzuken Memorial Foundation, and Hirao Taro Foundation of Konan Gakuen for Academic Research. A.K. was supported by the Asahi Glass Foundation, Mochida Memorial Foundation for Medical and Pharmaceutical Research, AMED PRIME (22gm6510004h0002), and JSPS KAKENHI (22H05512, 21H02534, 21K19279, and 20H05074). A.O. and H.M. were supported by JSPS KAKENHI (18K06344, 19J40017, and 21K06275 [A.O.], and 21J20026 [H.M.]).

Author affiliations: [a]Graduate School of Natural Science, Konan University, Kobe 658-8501, Japan; [b]Faculty of Science and Engineering, Konan University, Kobe 658-8501, Japan; [c]Institute for Integrative Neurobiology, Konan University, Kobe 658-8501, Japan; and [d]AMED-PRIME, Japan Agency for Medical Research and Development, Tokyo 100-0004, Japan

1. J. G. Boyles, F. Seebacher, B. Smit, A. E. McKechnie, Adaptive thermoregulation in endotherms may alter responses to climate change. *Integr. Comp. Biol.* **51**, 676–690 (2011).
2. M. J. Angilletta, Jr, J. P. Youngblood, L. K. Neel, J. M. VandenBrooks, The neuroscience of adaptive thermoregulation. *Neurosci. Lett.* **692**, 127–136 (2019).
3. A. Ohta, T. Ujisawa, S. Sonoda, A. Kuhara, Light and pheromone-sensing neurons regulates cold habituation through insulin signalling in *Caenorhabditis elegans*. *Nat. Commun.* **5**, 4412 (2014).
4. M. Okahata *et al.*, Natural variations of cold tolerance and temperature acclimation in *Caenorhabditis elegans*. *J. Comp. Physiol. B* **186**, 985–998 (2016).
5. M. Okahata, H. Motomura, A. Ohta, A. Kuhara, Molecular physiology regulating cold tolerance and acclimation of *Caenorhabditis elegans*. *Proc. Jpn. Acad. Ser. B Phys. Biol. Sci.* **98**, 126–139 (2022).
6. S. Sonoda, A. Ohta, A. Maruo, T. Ujisawa, A. Kuhara, Sperm affects head sensory neuron in temperature tolerance of *Caenorhabditis elegans*. *Cell Rep.* **16**, 56–65 (2016).
7. K. Ohnishi *et al.*, Molecular and cellular network systems underlying cold tolerance of *Caenorhabditis elegans*. *Cryobiol. Cryotechnol.* **64**, 53–59 (2018).
8. M. Okahata, A. D. Wei, A. Ohta, A. Kuhara, Cold acclimation via the KQT-2 potassium channel is modulated by oxygen in *Caenorhabditis elegans*. *Sci. Adv.* **5**, eaav3631 (2019).
9. K. Ohnishi *et al.*, OSM-9 and OCR-2 TRPV channels are accessorial warm receptors in *Caenorhabditis elegans* temperature acclimatisation. *Sci. Rep.* **10**, 18566 (2020).
10. N. Takagaki *et al.*, The mechanoreceptor DEG-1 regulates cold tolerance in *Caenorhabditis elegans*. *EMBO Rep.* **21**, e48671 (2020).
11. E. R. Kandel, The molecular biology of memory storage: A dialogue between genes and synapses. *Science* **294**, 1030–1038 (2001).
12. P. L. Greer, M. E. Greenberg, From synapse to nucleus: Calcium-dependent gene transcription in the control of synapse development and function. *Neuron* **59**, 846–860 (2008).
13. Y. Nishida, T. Sugi, M. Nonomura, I. Mori, Identification of the AFD neuron as the site of action of the CREB protein in *Caenorhabditis elegans* thermotaxis. *EMBO Rep.* **12**, 855–862 (2011).
14. A. Ohta, A. Kuhara, Molecular mechanism for trimetric G protein-coupled thermosensation and synaptic regulation in the temperature response circuit of *Caenorhabditis elegans*. *Neurosci. Res.* **76**, 119–124 (2013).
15. A. Takeishi, N. Takagaki, A. Kuhara, Temperature signaling underlying thermotaxis and cold tolerance in *Caenorhabditis elegans*. *J. Neurogenet.* **34**, 351–362 (2020).
16. M. L. Nonet, O. Saifee, H. Zhao, J. B. Rand, L. Wei, Synaptic transmission deficits in *Caenorhabditis elegans* synaptobrevin mutants. *J. Neurosci.* **18**, 70–80 (1998).
17. J. G. White, E. Southgate, J. N. Thomson, S. Brenner, The structure of the nervous system of the nematode *Caenorhabditis elegans*. *Philos. Trans. R. Soc. Lond. B Biol. Sci.* **314**, 1–340 (1986).
18. I. Mano, M. Driscoll, *Caenorhabditis elegans* glutamate transporter deletion induces AMPA-receptor/adenylyl cyclase 9-dependent excitotoxicity. *J. Neurochem.* **108**, 1373–1384 (2009).
19. D. Sieburth, J. M. Madison, J. M. Kaplan, PKC-1 regulates secretion of neuropeptides. *Nat. Neurosci.* **10**, 49–57 (2007).
20. J. Y. Sze, M. Victor, C. Loer, Y. Shi, G. Ruvkun, Food and metabolic signalling defects in a *Caenorhabditis elegans* serotonin-synthesis mutant. *Nature* **403**, 560–564 (2000).
21. E. R. Sawin, R. Ranganathan, H. R. Horvitz, *C. elegans* locomotory rate is modulated by the environment through a dopaminergic pathway and by experience through a serotonergic pathway. *Neuron* **26**, 619–631 (2000).

22. G. Garriga, C. Desai, H. R. Horvitz, Cell interactions control the direction of outgrowth, branching and fasciculation of the HSN axons of *Caenorhabditis elegans*. *Development* **117**, 1071–1087 (1993).
23. T. Ujisawa *et al.*, Endoribonuclease ENDU-2 regulates multiple traits including cold tolerance via cell autonomous and nonautonomous controls in *Caenorhabditis elegans*. *Proc. Natl. Acad. Sci. U.S.A.* **115**, 8823–8828 (2018).
24. L. Pereira *et al.*, A cellular and regulatory map of the cholinergic nervous system of *C. elegans*. *eLife* **4**, e12432 (2015).
25. R. Y. Lee, E. R. Sawin, M. Chalfie, H. R. Horvitz, L. Avery, EAT-4, a homolog of a mammalian sodium-dependent inorganic phosphate cotransporter, is necessary for glutamatergic neurotransmission in *Caenorhabditis elegans*. *J. Neurosci.* **19**, 159–167 (1999).
26. J. Dillon *et al.*, Metabotropic glutamate receptors: Modulators of context-dependent feeding behaviour in *C. elegans*. *J. Biol. Chem.* **290**, 15052–15065 (2015).
27. W. Zou *et al.*, Decoding the intensity of sensory input by two glutamate receptors in one *C. elegans* interneuron. *Nat. Commun.* **9**, 4311 (2018).
28. P. J. Brockie, A. V. Maricq, Ionotropic glutamate receptors in *Caenorhabditis elegans*. *Neurosignals* **12**, 108–125 (2003).
29. S. R. Taylor *et al.*, Molecular topography of an entire nervous system. *Cell* **184**, 4329–4347.e23 (2021).
30. A. Bhattacharya, U. Aghayeva, E. G. Berghoff, O. Hobert, Plasticity of the electrical connectome of *C. elegans*. *Cell* **176**, 1174–1189.e16 (2019).
31. P. Murray, S. A. Hayward, G. G. Govan, A. Y. Gracey, A. R. Cossins, An explicit test of the phospholipid saturation hypothesis of acquired cold tolerance in *Caenorhabditis elegans*. *Proc. Natl. Acad. Sci. U.S.A.* **104**, 5489–5494 (2007).
32. L. Palamiuc *et al.*, A tachykinin-like neuroendocrine signalling axis couples central serotonin action and nutrient sensing with peripheral lipid metabolism. *Nat. Commun.* **8**, 14237 (2017).
33. J. H. Lee *et al.*, Lipid droplet protein LID-1 mediates ATGL-1-dependent lipolysis during fasting in *Caenorhabditis elegans*. *Mol. Cell. Biol.* **34**, 4165–4176 (2014).
34. F. Liu, Y. Xiao, X. L. Ji, K. Q. Zhang, C. G. Zou, The cAMP-PKA pathway-mediated fat mobilization is required for cold tolerance in *C. elegans*. *Sci. Rep.* **7**, 638 (2017).
35. E. J. O'Rourke, A. A. Soukas, C. E. Carr, G. Ruvkun, *C. elegans* major fats are stored in vesicles distinct from lysosome-related organelles. *Cell Metab.* **10**, 430–435 (2009).
36. A. Kuhara, N. Ohnishi, T. Shimowada, I. Mori, Neural coding in a single sensory neuron controlling opposite seeking behaviours in *Caenorhabditis elegans*. *Nat. Commun.* **2**, 355 (2011).
37. T. Ujisawa, A. Ohta, M. Uda-Yagi, A. Kuhara, Diverse regulation of temperature sensation by trimeric G-protein signaling in *Caenorhabditis elegans*. *PLoS One* **11**, e0165518 (2016).
38. G. Esposito, E. Di Schiavi, C. Bergamasco, P. Bazzicalupo, Efficient and cell specific knock-down of gene function in targeted *C. elegans* neurons. *Gene* **395**, 170–176 (2007).
39. R. S. Kamath, J. Ahringer, Genome-wide RNAi screening in *Caenorhabditis elegans*. *Methods* **30**, 313–321 (2003).